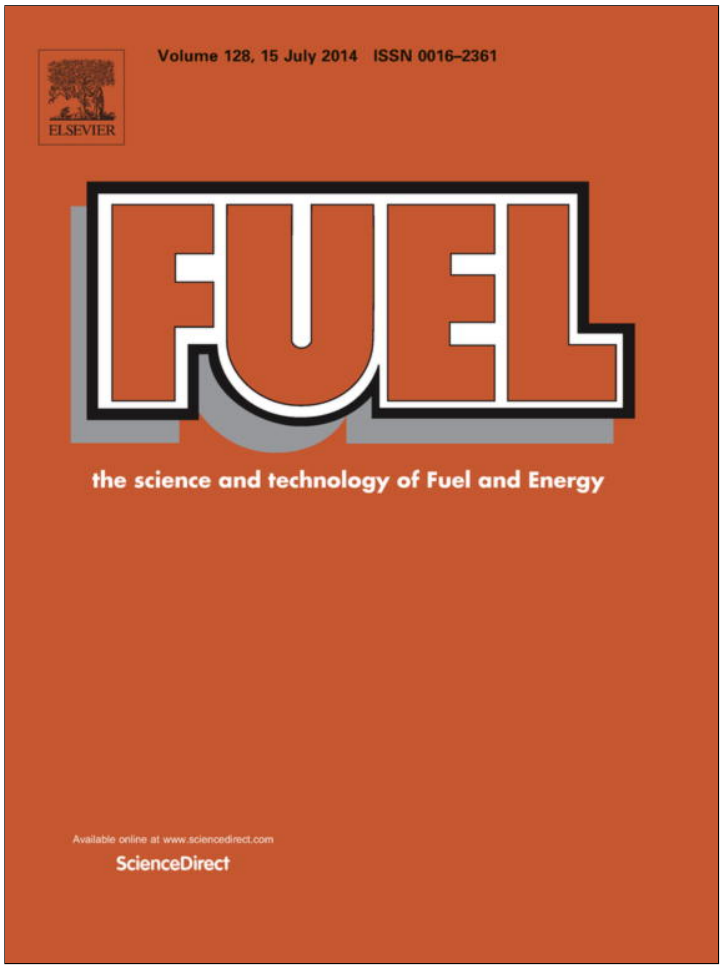

Fuel 128 (2014) 314–329

Contents lists available at ScienceDirect

Fuel

journal homepage: www.elsevier.com/locate/fuel

Ionic liquids for thiols desulfurization: Experimental liquid–liquid equilibrium and COSMO-RS description

Ana R. Ferreira [a,b], Mara G. Freire [a], Jorge C. Ribeiro [c], Fernando M. Lopes [c], João G. Crespo [b], João A.P. Coutinho [a,*]

[a] CICECO, Departamento de Química, Universidade de Aveiro, 3810-193 Aveiro, Portugal
[b] CQFB/REQUIMTE, Departamento de Química, FCT, Universidade Nova de Lisboa, 2829-516 Caparica, Portugal
[c] Galp Energia, Refinaria de Matosinhos, 4452-852 Leça da Palmeira, Matosinhos, Portugal

HIGHLIGHTS

- Liquid–liquid equilibrium phase diagrams for ionic liquid + thiol + *n*-alkane.
- Impact of the ionic liquid structural features in the extraction of 1-hexanethiol.
- High selectivities and low solute distribution ratios were obtained.
- Experimental validation of the COSMO-RS predictions.
- Extensive ionic liquids screening envisaging thiols extraction using COSMO-RS.

ARTICLE INFO

Article history:
Received 13 January 2014
Received in revised form 6 March 2014
Accepted 11 March 2014
Available online 21 March 2014

Keywords:
Desulfurization
Thiol
Aliphatic hydrocarbon
Ionic liquid
Liquid–liquid equilibrium
COSMO-RS

ABSTRACT

Aiming at the replacement of the present inefficient and expensive desulfurization processes, ionic liquids have been considered as potential solvents to be used in extraction procedures. In this context, this work provides an experimental evaluation on the feasibility of ionic liquids for the selective extraction of a less studied class of aliphatic sulfur compounds – thiols. A mixture composed of *n*-dodecane and 1-hexanethiol was used, as a feed model of kerosene in "jet-fuel", and the tie-lines of the corresponding ternary systems were experimentally determined at 298.2 K and 313.2 K for imidazolium- and pyridinium-based ionic liquids. Using the experimental data, the selectivity and distribution ratios of 1-hexanethiol were also determined. Despite the small distribution ratios, these systems display a high selectivity meaning that the co-extraction of other fuel compounds can be controlled by the ionic liquids nature and/or chemical structural characteristics. The COnductor-like Screening MOdel for Real Solvents (COSMO-RS) was used to predict the liquid–liquid equilibrium of the investigated systems. A good agreement between the experimental data and the COSMO-RS results was observed. Therefore, the extraction behavior with other ionic liquids not experimentally addressed was also predicted by COSMO-RS for the identification of the best potential candidates. The ionic liquids identified are constituted by a short alkyl side chain imidazolium, pyridinium and pyrrolidium cations, combined with the anions tosylate, diethylphosphate, ethylsulfate and triflate.

1. Introduction

Sulfur emissions from fossil fuels, coal and chemical burning, as well as by refinery industries have a great impact in human health and in the overall environment. The release of sulfur compounds is responsible for the production of SO_x, which additionally lead to acid rain, ozone depletion, and respiratory insufficiency in humans. Regarding the fuel use, SO_x is also responsible for the deactivation of automotive catalytic converters which further inhibit the performance of the pollution control equipment and lead to the release of additional toxic and volatile organic compounds. To minimize these major environmental and health concerns, the authorities implemented more strict policies where fuel sulfur limits have been drastically reduced to near-zero levels (<10 ppm S) [1,2].

Desulfurization is thus, today, one of the most important processes on a refinery. Commonly, the reduction of the sulfur content is attained through the conventional hydrodesulfurization process

* Corresponding author. Tel.: +351 234 401507; fax: +351 234 370084.
E-mail address: jcoutinho@ua.pt (J.A.P. Coutinho).

http://dx.doi.org/10.1016/j.fuel.2014.03.020
0016-2361/

(HDS). This treatment consists in the hydrogenation of the sulfur compound (aliphatics and aromatics) into hydrogen sulfides and hydrocarbons at elevated temperatures and high hydrogen pressure [1,2]. Despite the hydrocarbon recovery, there is also an octane number decrease by the saturation of olefins. However, this type of treatment represents high economic investments and operation costs. In addition, for the distilled branches with higher molecular weight sulfur-compounds, which present lower reactivity, more severe conditions are even required since these compounds are more difficult to hydrogenate, increasing therefore the operation costs [1,2]. The sulfur removal by the HDS process needs a quality upgrading of the existing technologies and a continuous development of new alternative desulfurization approaches. Various options were already considered, such as selective and/or oxidative extractions, reactive adsorption, biodesulfurization, membrane separation, among others [1–7].

Ionic liquids (ILs) belong to the molten salts group and are generally composed of bulky and asymmetric organic cations and organic or inorganic anions. Most ionic liquids exhibit desirable attributes, namely a negligible vapor pressure, a wide temperature range where they are liquid, high thermal and chemical stabilities, and a good solvating capacity for both organic and inorganic compounds, among others [8]. Therefore, ionic liquids appear as more attractive and competitive solvents compared to the conventional volatile organic solvents, especially due to their negligible vapor pressure and high thermal stability. Additionally, the huge number of possible ionic liquids that can be synthesized by a proper selection of the cation/anion combinations allows the tuning of their solvation ability for a variety of solutes. This tailoring feature makes possible to choose an ionic liquid that presents reduced solubility in the feed liquid phase and a high affinity for the target solute to be removed.

During the past few years, several research works have been addressing the use of ionic liquids for the removal of sulfur-based compounds from distilled streams, such as gasoline, kerosene and diesel [3,9–16]. These studies comprised different forms of desulfurization processes, and amongst them, it can be found the liquid–liquid extraction [16–25] and simultaneous oxidation [9,15,26–33], the oxidative extraction [32,34,35], and the use of supported ionic liquids in membranes or solid particles [14,36–38]. Most of the studies have focused on aromatic sulfur compounds (thiophene, benzothiophene, benzothiophene and their derivates) since they are present in higher contents in the refinery streams when compared with the aliphatic analogs. Wasserscheid et al. [14,39] studied the removal of *n*-butyl mercaptan from *n*-heptane and *n*-decane using imidazolium-phosphate-, chloride- and bis[(trifluoromethyl)sulfonyl]imide-based ionic liquids, either in simple liquid extractions or in absorptive processes using the ionic liquid immobilized in a ceramic support. The ethanethiol extraction from gasoline was proposed by Martínez-Palou et al. [40] and its interactions with both anhydrous Fe(III) chloride anions and 1-butyl-3-methylimidazolium-based ionic liquids were investigated.

Taking into account the scarcity of reported results concerning the removal of thiols [14,39,40], this work aims at studying the ionic liquids as potential extracting solvents for organosulfur compounds with the sulfhydryl group and a sided alkyl chain (R-SH), considering kerosene as the fuel fraction to be treated for the production of "jet-fuel". Though this hydrocarbon mixture is very complex, the "jet-fuel" model assumed here is a *n*-alkane, *n*-dodecane, and the thiol 1-hexanethiol. The liquid–liquid equilibrium for the ternary mixture composed of 1-hexanethiol, *n*-dodecane and several ionic liquids, based either on imidazolium or pyridinium cations, combined with the anions methylsulfate, methanesulfonate, triflate, bis(trifluoromethylsulfonyl)imide and tetrafluoroborate, was determined at 298.2 K and 313.2 K, and at atmospheric pressure. The large number of ionic liquids studied further allowed the understanding of the ionic liquid features that enhance the extraction of high molecular weight thiols.

Keeping in mind that the screening of the huge number of possible ionic liquids and hydrocarbons mixtures is experimentally unfeasible, the use of predictive models and/or computational methods is a viable option for the design of the best solvent. Thus, the COnductor-like Screening MOdel for Real Solvents (COSMO-RS) [41–43] was also employed to describe the liquid–liquid equilibria experimentally addressed aiming at evaluating its prediction performance. Albeit COSMO-RS was already applied in the description of equilibrium behavior of sulfur compounds, mainly aromatic sulfur compounds, with ionic liquid and hydrocarbon [44–55], the ability of COSMO-RS to describe the ternary systems comprising aliphatic sulfur compounds, is here assessed. Due to its fundamental nature, COSMO-RS only requires the information on the molecular structure of the compounds and has gained a spot place in the *a priori* prediction of phase behavior, activity coefficients and other thermophysical data [47,48,50,52,56–61].

Supported on the good agreement obtained between the experimental data and COSMO-RS results, the model was further used in the identification of other potential ionic liquids for the thiol extraction.

2. Materials and methods

2.1. Liquid–liquid equilibrium

The selection of the ionic liquids to be tested was carried out taking into account the mutual solubility between aliphatic/aromatic hydrocarbons and ionic liquids. Low mutual solubilities are required in order to minimize the solvent loss or the contamination of the hydrocarbon-rich sample. Besides these conditions it is also necessary to choose ionic liquids with a high selectivity and distribution ratio values for thiols. As demonstrated in our previous work [62], the cation side alkyl chain length of ionic liquids is the feature with the major impact within these system's miscibility. Longer alkyl side chains or the predominance of non-polar regions increases the dispersive interactions between the ionic liquid and the hydrocarbons which can lead to a significant loss of the feed. Therefore, the longest alkyl side chains of the ionic liquid cations studied here are ethyl and butyl to reduce the mutual solubility between the ionic liquid and the hydrocarbons. Both imidazolium- and pyridinium-based ionic liquids were evaluated. Others cations, such as alkylphosphoniums or alkylammoniums, were not tested due to their high miscibility with *n*-alkanes and aromatics hydrocarbons [62].

2.1.1. Materials

The *n*-dodecane and 1-hexanethiol were acquired from Sigma–Aldrich, 99% and 95% pure, respectively, and were used as received. The imidazolium-based ionic liquids investigated were: 1-ethyl-3-methylimidazolium methylsulfate ($[C_2mim][MeSO_4]$), 1-ethyl-3-methylimidazolium methanesulfonate ($[C_2mim][CH_3SO_3]$), 1-ethyl-3-methylimidazolium triflate ($[C_2mim][CF_3SO_3]$), 1-ethyl-3-methylimidazolium bis(trifluoromethylsulfonyl)imide ($[C_2mim][NTf_2]$), 1-ethyl-3-methylimidazolium tetrafluoroborate ($[C_2mim][BF_4]$), 1-butyl-3-methylimidazolium methylsulfate ($[C_4mim][MeSO_4]$), 1-butyl-3-methylimidazolium triflate ($[C_4mim][CF_3SO_3]$), and 1-butyl-3-methylimidazolium bis(trifluoromethylsulfonyl)imide ($[C_4mim][NTf_2]$). The pyridinium-based ionic liquids studied were: 1-ethyl-3-methylpyridinium methanesulfonate ($[C_2mpy][CH_3SO_3]$), 1-ethyl-3-methylpyridinium triflate ($[C_2mpy][CF_3SO_3]$), and 1-ethyl-3-methylpyridinium bis(trifluoromethylsulfonyl)imide ($[C_2mpy][NTf_2]$). The chemical structures of the studied ionic

liquids, divided by cations and anions, are depicted in Tables 1 and 2. All the ionic liquids were acquired from IoLiTec, Ionic Liquid Technology, Germany, with a purity level >99 wt%. Before use, the ionic liquids were dried and purified by heating (313.2 K) under moderate vacuum, and with constant stirring for a minimum of 24 h. The ionic liquid water content was determined by Karl-Fischer titration, using

Table 1
Abbreviations and chemical structures of the ionic liquids cations studied.

Abbreviation	Description	Chemical structure
$[C_2mim]^+$	1-Ethyl-3-methylimidazolium	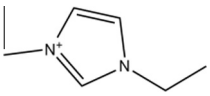
$[C_4mim]^+$	1-Butyl-3-methylimidazolium	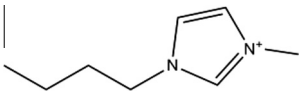
$[C_6mim]^+$	1-Hexyl-3-methylimidazolium	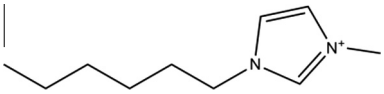
$[C_8mim]^+$	1-Methyl-3-octylimidazolium	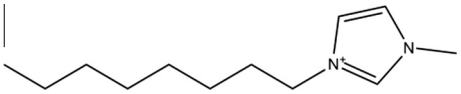
$[C_2C_2im]^+$	1,3-Diethylimidazolium	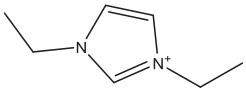
$[C_4C_4im]^+$	1,3-Dibutylimidazolium	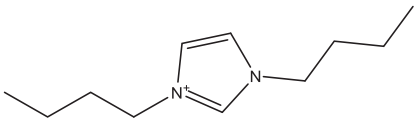
$[C_2mpy]^+$	1-Ethyl-3-methylpyridinium	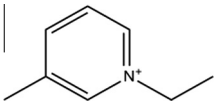
$[C_2mpyr]^+$	1-Ethyl-3-methylpyrrolidinium	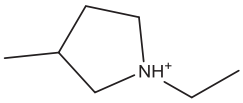
$[C_4iQuin]^+$	N-butyl-isoquinolinium	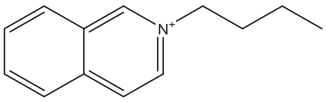
$[C_4TZO]^+$	3-Butyl-4-methylthiazolium	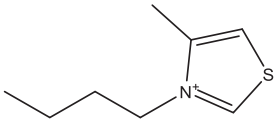
$[Ch]^+$	Ethyl(2-hydroxyethyl)dimethylammonium (cholinium)	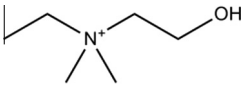
$[Gu]^+$	Guanidinium	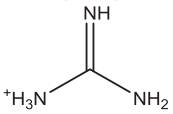
$[(C_1)_6Gu]^+$	Hexamethylguanidinium	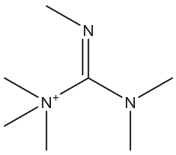
$[P_{666(14)}]^+$	Trihexyl(tetradecyl)phosphonium	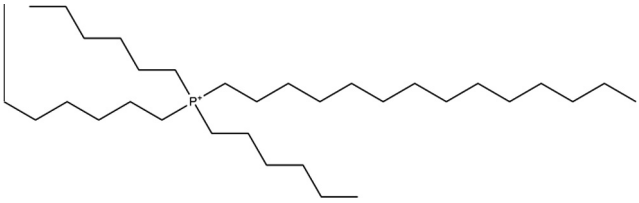

Table 1 (*continued*)

Abbreviation	Description	Chemical structure
$[OC_2(C_1)4iU]^+$	O-ethyl-N,N,N,N-tetramethylisothiouronium	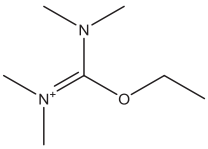
$[SC_2(C_1)4iU]^+$	S-ethyl-N,N,N,N-tetramethylisothiouronium	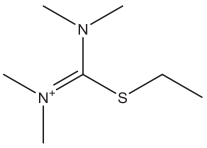

Table 2
Abbreviations and chemical structures of the ionic liquids anions studied.

Abbreviation	Description	Chemical structure
$[MeSO_4]^-$	Methylsulfate	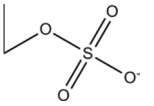
$[EtSO_4]^-$	Ethylsulfate	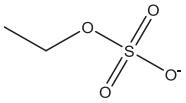
$[BuSO_4]^-$	Butylsulfate	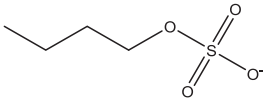
$[OcSO_4]^-$	Octylsulfate	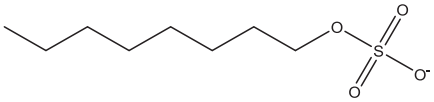
$[CH_3SO_3]^-$	Methylsulfonate	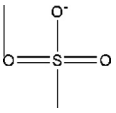
$[CF_3SO_3]^-$	Trifluoromethanesulfonate	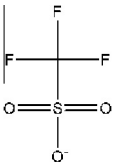
$[(PFBu)SO_3]^-$	Perfluorobutanesulfonate	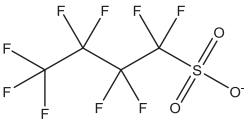
$[CH_3CO_2]^-$	Acetate	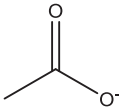
$[NTf_2]^-$	Bis[(trifluoromethyl)sulfonyl]imide	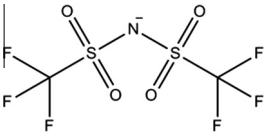
$[PF_6]^-$	Hexafluorophosphate	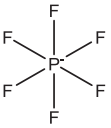
$[BF_4]^-$	Tetrafluoroborate	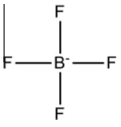

(*continued on next page*)

Table 2 (*continued*)

Abbreviation	Description	Chemical structure
$[N(CN)_2]^-$	Dicyanamide	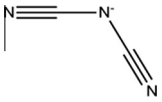
$[C(CN)_3]^-$	Tricyanomethane	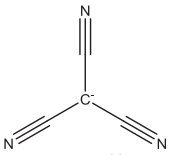
$[B(CN)_4]^-$	Tetracyanoborate	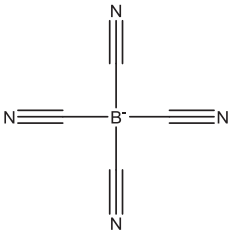
$[TOS]^-$	Tosylate	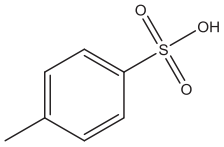
$[DEP]^-$	Diethylphosphate	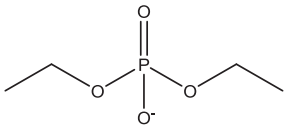
$[DBP]^-$	Dibutylphosphate	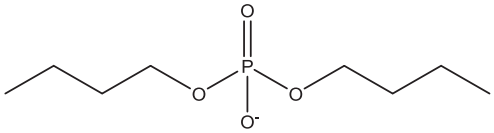
$[NO_3]^-$	Nitrate	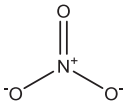
$[FeCl_4]^-$	Tetrachloroferrate	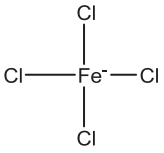

a Metrohm 831 Karl Fischer coulometer. The water content values are presented in Supporting information, Table S1.

2.1.2. Experimental procedure

The ionic liquids were selected present a very low solubility in the hydrocarbon under study (*n*-dodecane). All the ternary systems investigated present two distinct liquid phases, an upper phase rich in *n*-dodecane and a lower IL-rich phase. The 1-hexanethiol is partitioned between the two phases. As the real sulfur content in crude oils is very low, the measured equilibrium tie-lines correspond to the lowest region of the ternary phase diagram with the mole fraction of 1-hexanethiol ranging between 0.015 and 0.025 in the overall mixture composition.

The ternary mixtures were prepared in glass vials (10 mL) with screw caps to prevent the evaporation of volatile compounds as well as to avoid the adsorption of moisture from atmosphere. Known quantities of each component were weighed within 10^{-4} g (Precisa, model XT220A, Sweden), and added directly to the glass vials.

The ternary mixtures were stirred and left at rest for at least 24 h at the desired temperature (±0.5 K). When the equilibrium was attained two clear liquid phases were observed. After the equilibration, individual samples were carefully taken from the upper and bottom phases using syringes for further quantification.

The thiol, in each phase, was quantified by potentiometric titration, using a TitraLab® 865 titration workstation, with an alcoholic solution of $AgNO_3$ at 0.01 M, according to the ASTM D3227 standard [63]. The ionic liquid content in the hydrocarbon-rich phase was determined by UV spectroscopy, using a Helios α UV–Vis spectrophotometer from Thermo Scientific. However, it should be highlighted that no peaks corresponding to each ionic liquid were found in all the tested samples meaning that their concentration is below the lower detection limit of the equipment. Therefore, in all situations, the content of ionic liquid in the hydrocarbon-rich phase was considered as insignificant or null. The *n*-dodecane in the ionic-liquid-rich phase was determined gravimetrically ($\pm 10^{-4}$ g) after a drying process under vacuum in which the *n*-alkane and the thiol are removed. At this step, samples of circa 0.5 g were used. However, and as happened with the ionic liquids in the hydrocarbon-rich phase, the amount of *n*-dodecane in the ionic-liquid-rich phase was found to be negligible in all situations. In summary, the quantification of each

component in each layer allowed the determination of the corresponding tie-lines.

2.2. COSMO-RS theory

COSMO-RS [41,43,64–66] is a thermodynamic model capable of forecasting several thermophysical properties and the phase behavior of pure fluids and/or mixtures. This means that this model does not require *a priori* experimental data since it is based on a combination of the properties of individual atoms comprising each molecule or ions. COSMO-RS combines quantum chemical approaches, based on the dielectric continuum model known as COSMO (COnductor-like Screening MOdel), with statistical thermodynamics calculations.

In the COSMO calculations, the molecules are surrounded by a virtual conductor environment, and the interactions are considered to take place on segments of this perfect/ideal conductor interface [41,43,64,65] taking into account the electrostatic screening and the back-polarization of the solute molecule. Thus, the discrete surface around the solute molecule and each segment are characterized by their geometry and screening charge density (σ), at a minimum energetic state of the conductor, stored in the so-called COSMO files. The complete description of the molecule is achieved by a distribution function designed by σ-profile $p_S(\sigma)$, that describes the molecular interactions [65].

Additionally, COSMO-RS considers three specific interaction energies, described as a function of the polarization charges of the two interacting segments – (σ, σ') or $(\sigma_{acceptor}, \sigma_{donor})$:

– Electrostatic misfit energy:

$$E_{MF}(\sigma,\sigma') = a_{eff}\frac{\alpha'}{2}(\sigma+\sigma')^2 \tag{1}$$

– Hydrogen-bonding energy:

$$E_{HB} = a_{eff}c_{HB}\min(0;\min(0;\sigma_{donor}+\sigma_{HB})\times\max(0;\sigma_{acceptor}-\sigma_{HB})) \tag{2}$$

– Van der Waals energy:

$$E_{vdW} = a_{eff}(\tau_{vdW}+\tau'_{vdW}) \tag{3}$$

where a_{eff} is the effective contact area between two surface segments, α' is an interaction parameter, c_{HB} is the hydrogen-bond strength, (σ_{HB}) is the threshold for hydrogen-bonding, and τ_{vdW} and τ'_{vdW} are element specific van der Waals interaction parameters.

The σ-potential, $\mu_S(\sigma)$ and the pseudo-chemical potential of the component X_i in a solvent S, $\mu_S^{X_i}$, calculated by Eqs. (4) and (5) [65], allow the prediction of several thermodynamic properties and phase behavior, such as the activity coefficient, distribution ratio, and phase equilibrium, among others [43,58,59,64,65].

$$\mu_S(\sigma) = -\frac{RT}{a_{eff}}\ln\left[\int p_S(\sigma')\times\exp\left(\frac{1}{RT}(a_{eff}\mu_S(\sigma')-E_{misfit}(\sigma,\sigma')-E_{HB}(\sigma,\sigma'))\right)d\sigma'\right] \tag{4}$$

$$\mu_S^{X_i} = \mu_{C,S}^{X_i} + \int p^{X_i}(\sigma)\mu_S(\sigma)d\sigma \tag{5}$$

All the COSMO-RS calculations were carried out with the lower energy state of the conformers of each ionic liquid anion and cation. This approach was defined according to the results by Freire et al. [58] showing that the best results are obtained using the lowest energetic conformers. The quantum chemical COSMO calculation was performed in the Turbomole program package [67] with the BP density functional theory, giving the surface charge density and the Ahlrichs-TZVP (triple-ζ valence polarized large basis set) [68]. The ternary liquid–liquid equilibria were estimated employing the COSMOtherm program using the parameter file BP_TZVP_C2.1_1301 [69].

3. Results and discussion

The phase equilibrium studies carried out in this work intent to support the selection of the most suitable ionic liquids for the extraction of sulfur compounds from hydrocarbon's streams by understanding of the effect of the ionic liquids nature and/or chemical structure on the ternary systems behavior.

Besides the determination of the corresponding tie-lines, the feasibility of the liquid–liquid extraction of 1-hexanethiol from the dodecane-rich layer using ionic liquids was further evaluated by the solvent selectivity (S) and distribution ratio (D) values. These parameters provide a quantitative description of the partitioning behavior of the thiol between the coexisting phases and can be determined according to the following equations:

$$S = \frac{\frac{x_{RSH}^{II}}{x_{HC}^{II}}}{\frac{x_{RSH}^{I}}{x_{HC}^{I}}} \tag{6}$$

$$D = \frac{x_{RSH}^{II}}{x_{RSH}^{I}} \tag{7}$$

where x is the mole fraction and the subscripts *RSH* and *HC* correspond to 1-hexanethiol and to the aliphatic hydrocarbon *n*-dodecane, respectively. The superscript I refers to the dodecane-rich-phase (upper phase), while II refers to the ionic-liquid-rich phase (bottom phase).

3.1. Ternary liquid–liquid equilibrium (tie-lines data)

The experimental liquid–liquid equilibrium (LLE) results are presented in Table S1, in the Supporting Information, and are plotted in Figs. 1–4. The tie-line data are plotted in an orthogonal ternary phase diagram, in which the *n*-dodecane was omitted, for a better visualization of the low experimental mole fraction values. In all the phase diagrams, the feed overall composition and the two equilibrium phase compositions are represented.

The ternary LLE obtained here are of type 2 [70], and which consist of two pairs of partially miscible components, namely 1-hexanethiol + *n*-dodecane and 1-hexanethiol + ionic liquid pairs. The binodal curves appear adjacent to the diagram axes; this trend is indicative of large immiscible regions mainly resulting from the very low mutual solubility between the ionic liquid and *n*-dodecane. Moreover, and as experimentally observed in the studied concentration ranges, no ionic liquid or *n*-dodecane were detected in the respective dodecane- and ionic-liquid-rich phases.

3.2. Selectivity and distribution ratio

For a better understanding of the influence of the ionic liquid structural characteristics through the selectivity and distribution ratio values for 1-hexanethiol, the following discussion is presented in different sections. The comparison between the different systems is expressed in distribution ratio, instead of using the LLE data, due to its overlapping values and undistinguishable differences in the ternary phase diagrams. Accordingly, using the experiments here carried out, the distribution ratio values are depicted in Figs. 5–9, divided by the effect of the cation core (Fig. 5), cation alkyl chain length (Fig. 6), anion nature (Fig. 7), temperature (Fig. 8) and water content (Fig. 9), as a function of the 1-hexanethiol concentration (mole fraction) in the dodecane-rich phase.

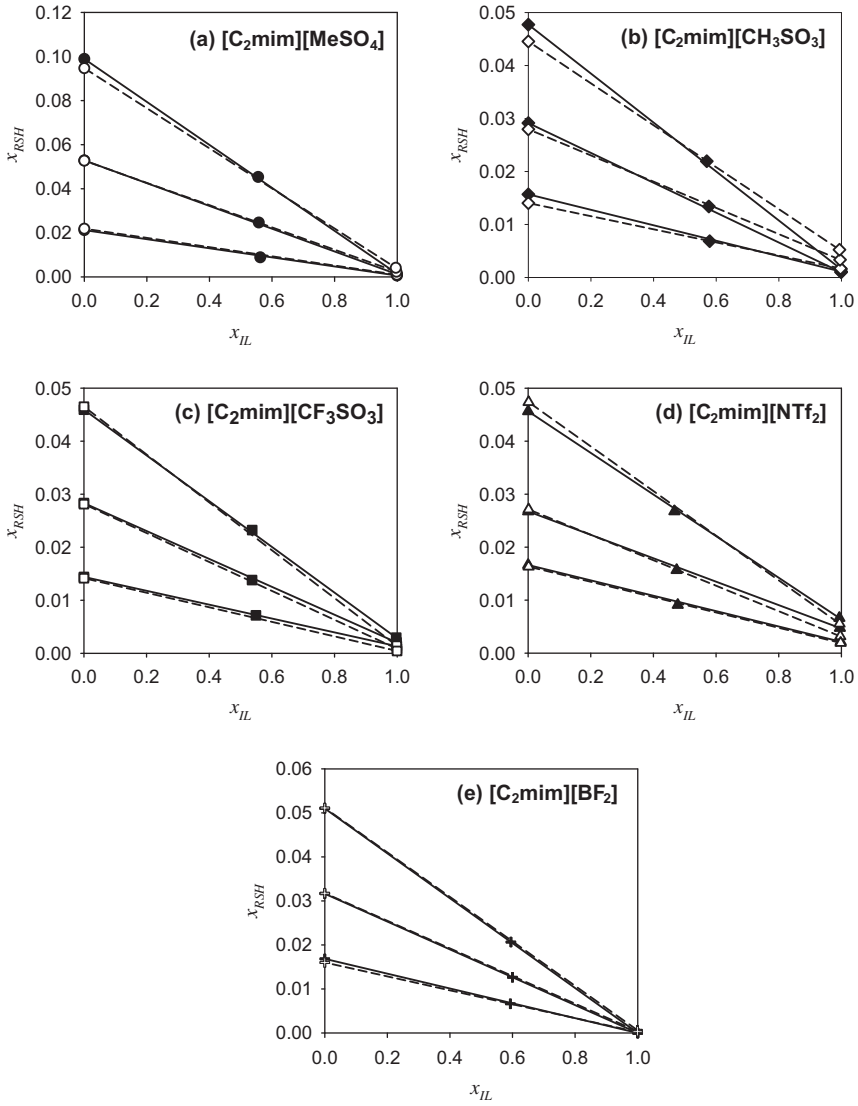

Fig. 1. Experimental and COSMO-RS predicted tie-lines for the LLE of ternary systems composed of [C_2mim]-based ionic liquids + 1-hexanethiol + *n*-dodecane (full symbols and solid lines for experimental data, and empty symbols and dashed lines for COSMO-RS predicted values), at 298.2 K and atmospheric pressure.

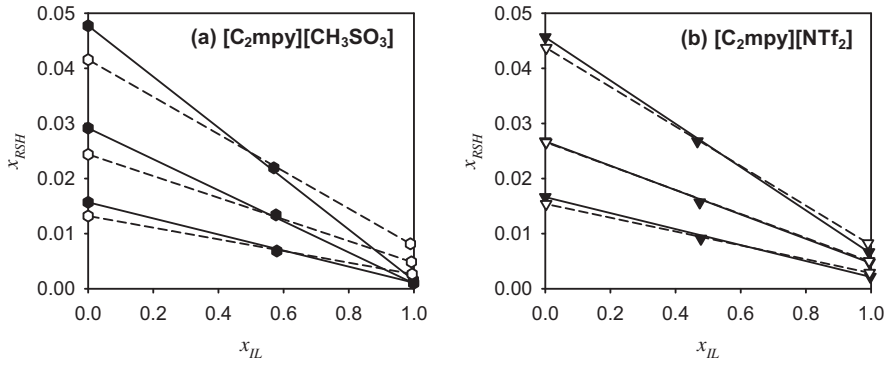

Fig. 2. Experimental and COSMO-RS predicted tie-lines for the LLE of ternary systems composed of [C_2mpy]-based ionic liquids + 1-hexanethiol + *n*-dodecane (full symbols and solid lines for experimental data, and empty symbols and dashed lines for COSMO-RS predicted values), at 298.2 K and atmospheric pressure.

In face of the negligible mutual solubilities between the studied ionic liquids and *n*-dodecane (Figs. 1–4), the selectivity of the ionic liquids for the thiol is almost complete while minimizing the loss of the ionic liquid and the contamination of the hydrocarbon stream. This trend represents a clear evidence of the ionic liquids potential for the extraction of thiols from hydrocarbon streams. On the other hand, the low distribution ratio values are related with the low affinity of the thiol for the ionic liquid and reflected by the negative tie-line slopes in the ternary phase diagrams. Regarding the selectivity and distribution ratio criteria, all the

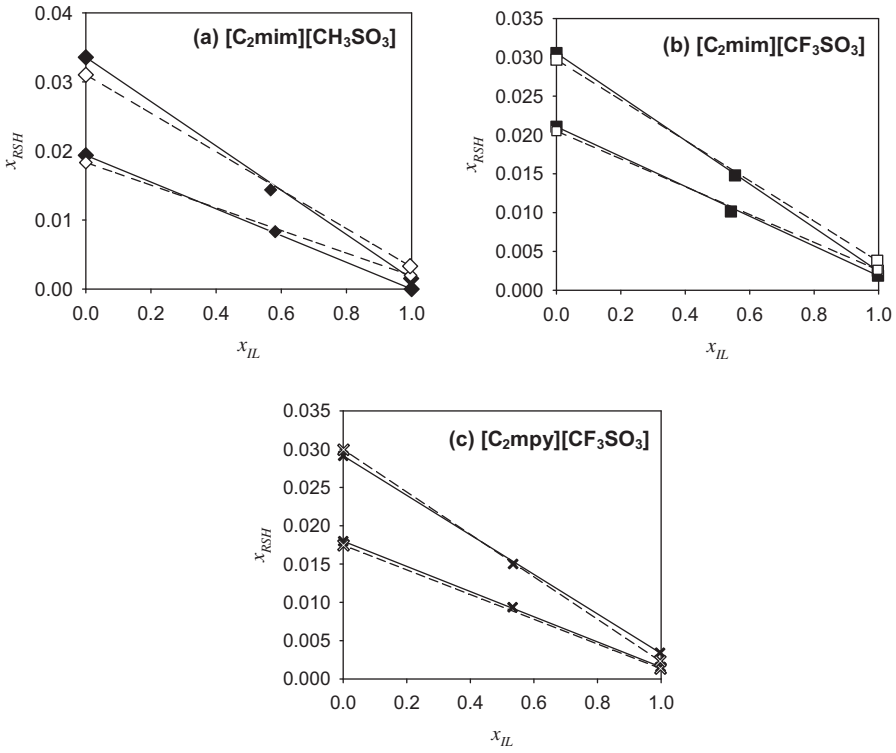

Fig. 3. Experimental and COSMO-RS predicted tie-lines for the LLE of ternary systems composed of ionic liquids + 1-hexanethiol + *n*-dodecane (full symbols and solid lines for experimental data, and empty symbols and dashed lines for COSMO-RS predicted values), at 313.2 K and atmospheric pressure.

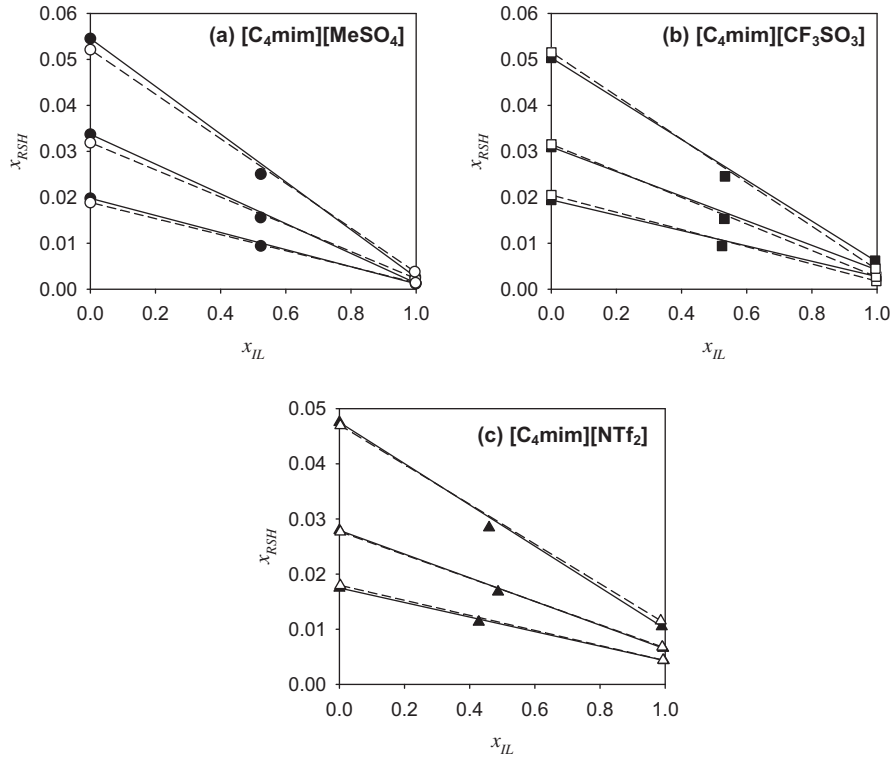

Fig. 4. Experimental and COSMO-RS predicted tie-lines for the LLE of ternary systems composed of [C_4mim]-based ionic liquids + 1-hexanethiol + *n*-dodecane (full symbols and solid lines for experimental data, and empty symbols and dashed lines for COSMO-RS predicted values), at 298.2 K and atmospheric pressure.

studied ternary systems display a similar behavior: high selectivity ($S \gg 1$) and distribution ratio lower than unit ($K \ll 1$). The weak interaction between 1-hexanethiol and imidazolium- or pyridinium-based ionic liquids can be explained by the different types of intermolecular forces that occur in the mixture. While thiols' interactions essentially comprise dispersion forces and less prominent dipole–dipole interactions between the individual –SH groups, the ionic liquids mainly present electrostatic and

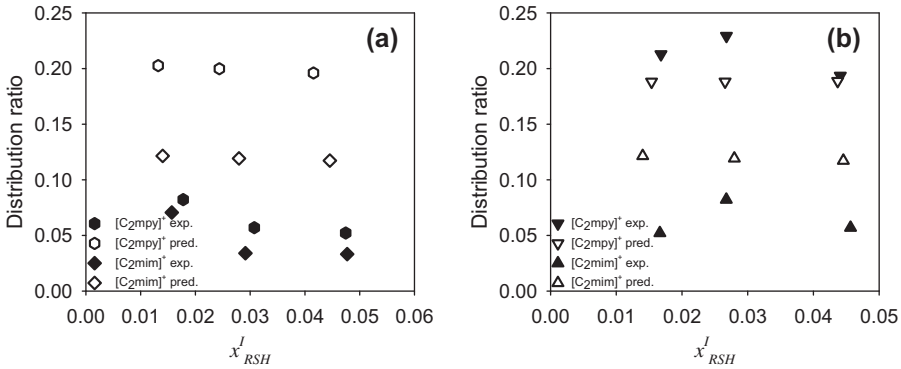

Fig. 5. Experimental and COSMO-RS predicted distribution ratio of1-hexanethiol in the ternary systems: (a) [cation][CH_3SO_3] + 1-hexanethiol + *n*-dodecane; and (b) [cation][NTf_2] + 1-hexanethiol + *n*-dodecane, at 298.2 K and atmospheric pressure.

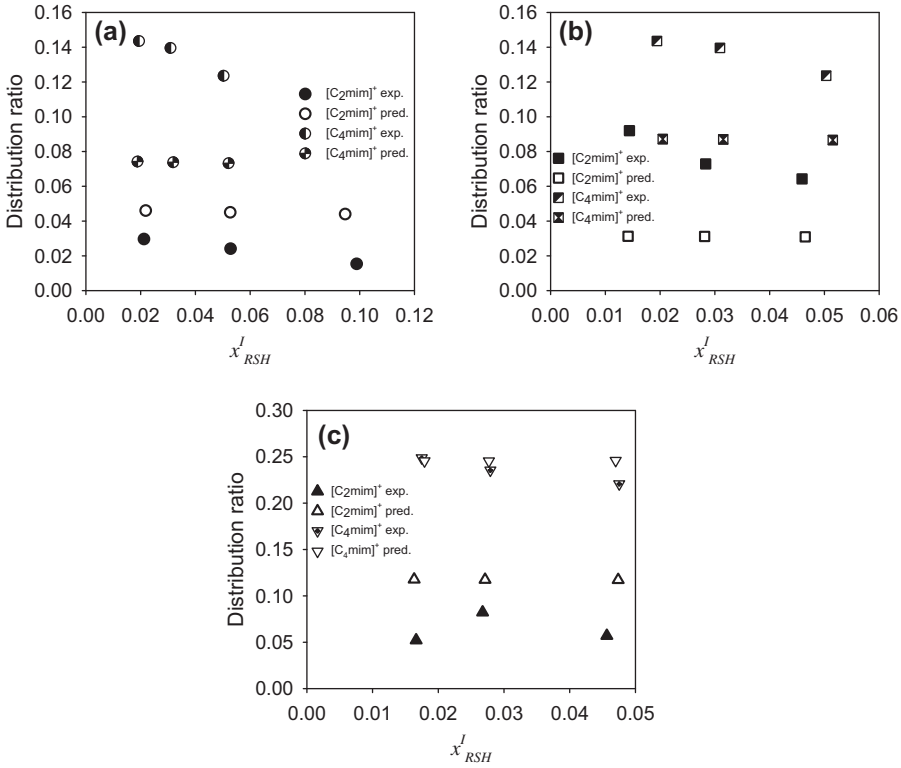

Fig. 6. Experimental and COSMO-RS predicted distribution ratio of 1-hexanethiol in the ternary systems: (a) [$C_n$mim][$MeSO_4$] + 1-hexanethiol + *n*-dodecane; (b) [$C_n$mim][CF_3SO_3] + 1-hexanethiol + *n*-dodecane; and (c) [$C_n$mim][NTf_2] + 1-hexanethiol + *n*-dodecane, at 298.2 K and atmospheric pressure.

hydrogen-bonding type interactions. Thus, the intermolecular interactions which could exist between both types of compounds are mainly van der Waals and dipole–dipole interactions. Since the tested ionic liquids have a short alkyl chain length the dispersive forces between the two compounds are small. The dipole–dipole attractions are also weak since the electronegativity difference between sulfur and hydrogen is low, making the S–H bond less polar than –OH, –NH or –FH bonds, where the hydrogen is bounded to highly electronegative atoms. Therefore, it is expectable that ion–thiol interactions are weaker than ion–ion or thiol–thiol interactions.

3.2.1. Effect of the ionic liquid cation core

Fixing the ionic liquid anion, it is possible to study the influence of the ionic liquid cation core on the distribution ratio of 1-hexanethiol towards the ionic-liquid-rich layer. Fig. 5a and b cover the common anions $[CH_3SO_3]^-$ and $[NTf_2]^-$, respectively, and allow the study of the effect of the imidazolium and the pyridinium cations. In both examples, the distribution ratio for the pyridinium-based systems is higher than for the imidazolium-based and which corresponds to a higher affinity of thiol for the first type of systems. For the fixed anion $[CH_3SO_3]^-$, the imidazolium-based system shows a distribution ratio of circa 0.05 whereas for the pyridinium cation it is 0.07. For the $[NTf_2]^-$ anion, the distribution ratio ranges from 0.06, for the imidazolium-based compound, to 0.21 for the pyridinium-based ionic liquid. Both cations are aromatic meaning that the higher affinity of 1-hexanethiol for the pyridinium-based ionic liquids should be related with its larger ring size. The pyridinium cation is a six-sided ring (Table 1), which being larger than the imidazolium five-sided ring, suffers a higher ring deformation by the charge density delocalization [71]. This delocalization of charge contributes to an increase in the van der Waals interactions between the thiol and the ionic liquid cation.

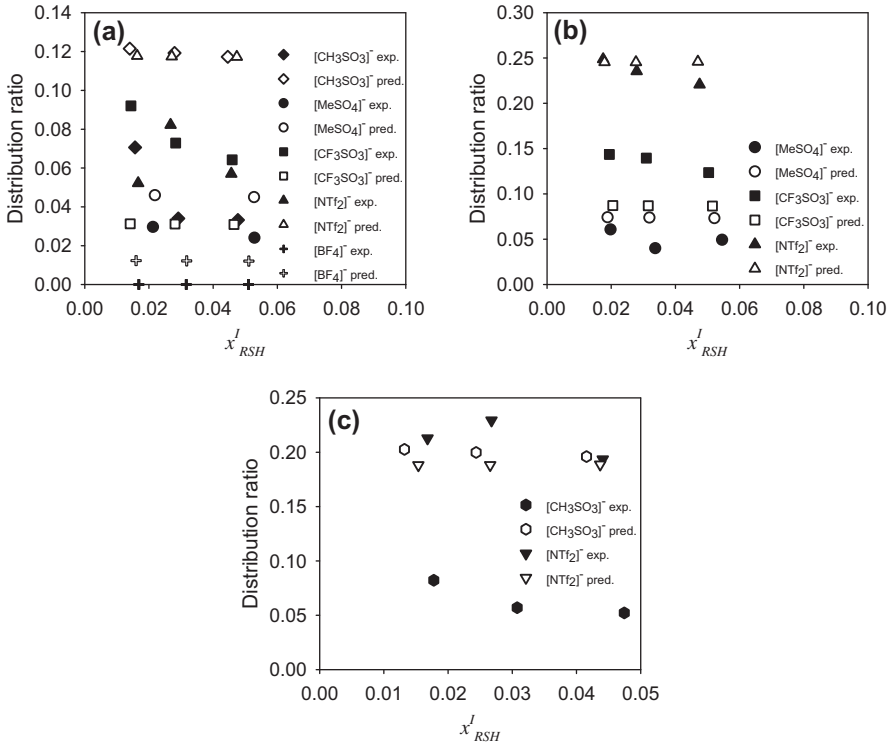

Fig. 7. Experimental and COSMO-RS predicted distribution ratio of 1-hexanethiol in the ternary systems: (a) [C_2mim][anion] + 1-hexanethiol + *n*-dodecane; (b) [C_4mim][anion] + 1-hexanethiol + *n*-dodecane; and (c) [C_2mpy][anion] + 1-hexanethiol + *n*-dodecane, at 298.2 K and atmospheric pressure.

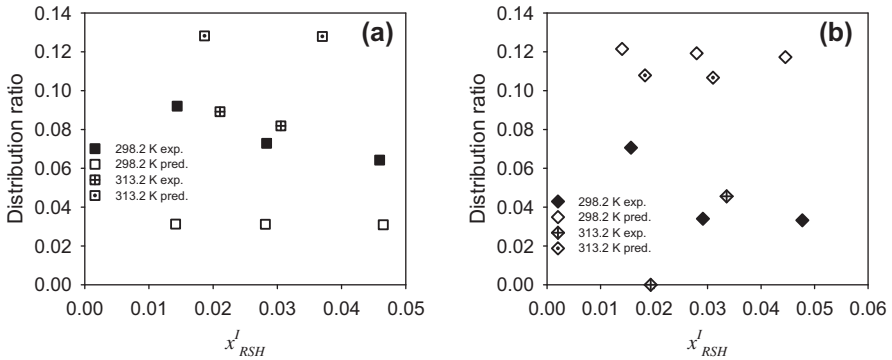

Fig. 8. Experimental and COSMO-RS predicted distribution ratio of 1-hexanethiol in the ternary systems: (a) [C_2mim][CF_3SO_3] + 1-hexanethiol + *n*-dodecane, and (b) [C_2mim][CH_3SO_3] + 1-hexanethiol + *n*-dodecane, at the temperatures 298.2 K and 313.2 K, and atmospheric pressure.

A significant aspect also observed when comparing the distribution ratio data is that they are more pronounced in the [NTf_2]-based ionic liquids than for the $[CH_3SO_3]^-$ analogs. This reveals the importance of the anion, that has a highly impact on the systems behavior, not only due to its nature, but that is reflected in the cation–anion interaction strength [71,72]. Coulombic attractions and hydrogen-bonding can be so strong that they attenuate the cation–thiol interactions. These type of interactions are dependent on the radius and polarity of the anion and on the electronegativity of the atom with which the hydrogen bond is formed. In this way, a decrease in the anion charge density reflects a weaker interaction between the ionic liquid ions. $[NTf_2]^-$ is a non-polar anion whereas $[CH_3SO_3]^-$ is polar. Therefore, the cation–anion interactions are stronger for $[CH_3SO_3]^-$ [71,72]. In this case the ionic liquid cation is less available to interact with the thiol compound, leading to smaller variations in the distribution ratio when the cation is replaced.

It is also noteworthy to highlight that the influence of the cation family can be significantly distinct of the one presented in this work and that other structural cations should be considered for a more complete analysis.

3.2.2. Effect of cation alkyl side chain length

The length of the aliphatic moiety in the ionic liquid cation is a very important characteristic regarding the mutual solubilities between ionic liquids and hydrocarbons [62]. The impact of the alkyl side chain length in imidazolium-based ionic liquids is illustrated in Fig. 6a–c for the $[MeSO_4]^-$, $[CF_3SO_3]^-$ and $[NTf_2]^-$ anions. It is shown that an increase in the alkyl chain length from $[C_2mim]^+$ to $[C_4mim]^+$ results in an increase of the distribution ratio due to more favorable interactions between 1-hexanethiol and the ionic liquids. Longer aliphatic moieties increment the non-polar region of the cation, resulting in a more diffusive charge density, which slightly improves the dispersive interactions that take place

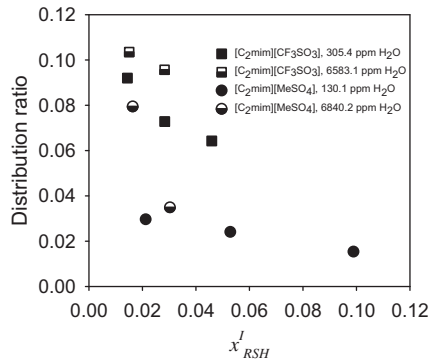

Fig. 9. Experimental distribution ratio of 1-hexanethiol in the ternary systems [C_2mim][$MeSO_4$] + 1-hexanethiol + *n*-dodecane with ionic liquid water content of 130 ppm, and 6840 ppm H_2O; and [C_2mim][CF_3SO_3] + 1-hexanethiol + *n*-dodecane with ionic liquid water content of 305 ppm, and 6583 ppm H_2O, at 298.2 K and atmospheric pressure.

between the thiol and the ionic liquids. For longer alkyl chains, an additional effect can also be expected by the increase of the free volume that allows a more efficient packing of the thiol on the cation–anion network. In addition, and as observed before with the cation core analysis, the effect of the alkyl side chain length is also influenced by the diverse ionic liquid anions. The most significant variation on the distribution ratios occurs for the weaker cation–anion interactions in [NTf_2]-based ionic liquids [71,72].

3.2.3. Effect of the ionic liquid anion nature

To further evaluate the effect associated with the anion nature, the distribution ratio of is presented in Fig. 7a–c. Fig. 7a, for the [C_2mim]-based ionic liquids, reveals an increase on the distribution ratio following the order: $[BF_4]^- < [MeSO_4]^- < [CH_3SO_3]^- < [CF_3SO_3]^- \sim [NTf_2]^-$, and ranging from 0 to 0.11. For the $[C_4mim]^+$ cation (Fig. 7b), the trend follows the rank: $[MeSO_4]^- < [CF_3SO_3]^- < [NTf_2]^-$. In the previous example, the distribution ratio varies from 0.04 to 0.25 since the alkyl chain is slightly longer and additional interactions can occur. The results for the [C_2mpy]-based ionic liquids combined with the $[CH_3SO_3]^-$ and $[NTf_2]^-$ anions are compared in Fig. 7c. The variation in the distribution ratio values obtained is also large ranging from 0.05 to 0.23. The higher distribution ratio values occur in the [NTf_2]-based ionic liquids. Thiol–anion interactions are mainly due to weak dispersive forces and the dependency behavior with the anions nature strongly ensues from their polarity. In this way, with the exception of the $[BF_4]^-$ anion, the experimental trend on the distribution ratio values closely follows the dipolarity/polarisability solvatochromic parameter (π^*) in [C_4mim]-based ionic liquids: $[MeSO_4]^- > [CH_3SO_3]^- > [BF_4]^- > [CF_3SO_3]^- > [NTf_2]^-$ [73].

3.2.4. Effect of the temperature

Aiming at the improvement of the distribution ratio of the systems composed of ionic liquid + 1-hexanethiol + *n*-dodecane, the effect of temperature in the LLE was also evaluated for the ionic liquids [C_2mim][CH_3SO_3] and [C_2mim][CF_3SO_3]. The distribution ratio values for both ionic liquids at 298.2 K and 313.2 K are plotted in Fig. 8a and b. The increase of temperature from 298.2 K to 313.2 K does not lead to enhanced distribution ratios. This behavior denotes that ionic liquids, for the extraction of thiols, can be used at temperatures close to room temperature without losing their performance. A separation process using ionic liquids at mild operational conditions and with lower energy costs is thus conceivable when compared to the traditional hydrodesulfurization process.

3.2.5. Effect of the ionic liquid water content

Since ionic liquids are highly hygroscopic, the water content has an important role in their thermophysical properties and phase behavior [74–76]. Therefore, the ionic liquids [C_2mim][$MeSO_4$] and [C_2mim][CF_3SO_3] with different water contents were also tested and the distribution ratio values were compared. The results obtained are shown in Fig. 9. An increase in the water content from 130.1 ppm and 305.4 ppm to 6840.2 ppm and 6583.1 ppm, for the [C_2mim][$MeSO_4$] and [C_2mim][CF_3SO_3] ionic liquids, respectively, was studied. From the results depicted in Fig. 9, the increase in the water content leads to an increase in the distribution ratio of 1-hexanethiol. Thus, the ionic liquid moisture adsorption can be seen as advantageous in the process separation at industrial scale.

3.3. Evaluation of the COSMO-RS prediction capability

The ionic liquids and conditions experimentally investigated allowed the understanding of the influence of the ionic liquid ions nature and temperature upon the phase behavior. Therefore, these data can be used to evaluate the predictive ability of COSMO-RS.

Along with the LLE experimental data (Figs. 1–4) and the distribution ratio results (Figs. 5–8), the COSMO-RS predicted values are also represented.

The COSMO-RS aptitude to describe the LLE results was also evaluated by the root mean square deviation (RMSD) to the experimental data. The RMSD is defined by the following equation:

$$\mathrm{RMSD} = \left[\sum_i \sum_n \left(x_{i,n}^{pred.I} - x_{i,n}^{\exp .I}\right)^2 + \left(x_{i,n}^{pred.II} - x_{i,n}^{\exp .II}\right)^2 \Big/ (2 \times N \times R)\right]^{1/2} \times 100 \quad (8)$$

where x is the mole fraction of compound i, R is the total number of compounds ($R = 3$), n is the tie-line number, and N is the total number of experiments. The RMSD values are listed in Table 3.

The results obtained with COSMO-RS for the tie-lines description (Figs. 1–4) are in good agreement with the experimental data. The low relative deviations presented in Table 3 between the predicted and experimental values also support this statement. The relative deviations vary from 0.04% to 0.8%, for the systems containing 1-hexanethiol in the mole fraction between 0.015 and 0.025, and in the overall mixture composition with *n*-dodecane. It is also visible that the RMSD values depend on the anion, and the ability of COSMO-RS to describe the liquid–liquid phase behavior of systems decreases with the anion polarity. Nonetheless, the low RMSD values achieved confirm the good performance of the COSMO-RS model on describing, quantitatively and qualitatively,

Table 3
Root mean square deviation (RMSD) between the compositions predicted by the COSMO-RS model and the experimental data for the ternary phase diagrams studied.

Ternary system: ionic liquid + 1-hexanethiol + *n*-dodecane	RMSD %
[C_2mim][$MeSO_4$] at 298.2 K	0.2
[C_2mim][CH_3SO_3] at 298.2 K	0.2
[C_2mim][CF_3SO_3] at 298.2 K	0.07
[C_2mim][NTf_2] at 298.2 K	0.1
[C_2mim][BF_4] at 298.2 K	0.04
[C_4mim][$MeSO_4$] at 298.2 K	0.1
[C_4mim][CF_3SO_3] at 298.2 K	0.1
[C_4mim][NTf_2] at 298.2 K	0.2
[C_2mim][CH_3SO_3] at 313.2 K	0.8
[C_2mim][CF_3SO_3] at 313.2 K	0.08
[C_2mpy][CH_3SO_3] at 298.2 K	0.5
[C_2mpy][NTf_2] at 298.2 K	0.2
[C_2mpy][CF_3SO_3] at 313.2 K	0.07

systems containing ionic liquids and hydrocarbon mixtures. These results allow the use of COSMO-RS for a quick and easy screening of the vast number of ionic liquid and hydrocarbon combinations.

The COSMO-RS predictive ability was also analyzed individually regarding the several aspects that can influence the behavior of systems constituted by ionic liquid + 1-hexanethiol + *n*-dodecane. The differences in the phase behavior by the change of the imidazolium cation for the pyridinium cation (Fig. 5), and also by the increase of the alkyl side chain length in the imidazolium cation (Fig. 6), in systems with the $[MeSO_4]^-$, $[CH_3SO_3]^-$, $[CF_3SO_3]^-$, and $[NTf_2]^-$ anions, is well described by COSMO-RS. However, and as previously observed for the binary phase behavior of ionic liquid + water systems [57], better predictions are obtained for the systems with the ionic liquids containing the less polar anions.

Taking into account the lower ability of COSMO-RS to predict the phase behavior of systems composed of ionic liquids with more polar anions, it is thus expectable a poorer performance of COSMO-RS to predict the influence of the anion nature on the liquid–liquid equilibrium (Fig. 7). Even though, the COSMO-RS results correctly correlate with the anion influence in the distribution ratio values, as depicted in Fig. 7b), better results are achieved for the $[C_4mim]$-based ionic liquids due to a decrease on the cation–anion interactions by the increase of the cation alkyl side chain from ethyl to butyl.

The minor increase on the distribution ratio with the increase on temperature from 298.2 K to 313.2 K is well predicted for the system containing $[C_2mim][CF_3SO_3]$. However, some disagreement is observed in the ternary system with $[C_2mim][CH_3SO_3]$ (Fig. 8a and b). Once again, a better description is obtained by COSMO-RS when dealing with more hydrophobic anions such as triflate.

4. Ionic liquid screening

COSMO-RS has been widely used in the modeling and prediction of many properties of systems comprising ionic liquids and petroleum constituents, such as aromatic and aliphatic hydrocarbons [60–62], as well as nitrogen and sulfur-based compounds [47,77]. Taking into account the evaluation carried out in this work on the COSMO-RS capability to predict the phase behavior of systems containing ionic liquids, thiols and alkanes, this model was used in the screening of a vaster number of ionic liquids with the goal of identifying the best candidates for the extraction of thiols.

4.1. Tested ionic liquids

The ternary systems evaluated are composed of an ionic liquid, a thiol (1-hexanethiol) and a *n*-alkane (*n*-dodecane). Around 280 ionic liquids were tested by the combination of 16 cations and 19 anions available on the COSMO-RS database. The cations investigated belong to very distinctive families and are: 1-ethyl-3-methylimidazolium, 1-butyl-3-methylimidazolium, 1-hexyl-3-methylimidazolium, 1-methyl-3-octylimidazolium, 1,3-diethyllimidazolium, 1,3-dibutyllimidazolium, 1-ethyl-3-methylpyridinium, 1-ethyl-3-methylpyrrolidinium, N-butyl-isoquinolinium, 3-butyl-4-methylthiazolium, cholinium (ethyl(2-hydroxyethyl)dimethylammonium), guanidinium, hexamethylguanidinium, trihexyl(tetradecyl)phosphonium, O-ethyl-N,N,N,N-tetramethylisothiouronium and S-ethyl-N,N,N,N-tetramethylisothiouronium. Furthermore, the anions tested are methylsulfate, ethylsulfate, butylsulfate, octylsulfate, methylsulfonate, trifluoromethanesulfonate (triflate), perfluorobutanesulfonate, acetate, bis[(trifluoromethyl)sulfonyl]imide, hexafluorophosphate, tetrafluoroborate, dicyanamide, tricyanomethanide, tetracyanoborate, tosylate, diethylphosphate, dibutylphosphate, nitrate and tetrachloroferrate. The anions/cations chemical structures and respective abbreviations are presented in Tables 1 and 2.

4.2. Selectivity, distribution ratio and σ-profiles

The ionic liquids screening was performed based on the predicted selectivity and distribution ratio with circa 2 mol/mol% of thiol present at the alkane-rich phase. Additionally, the estimated COSMO-RS energies and σ-profiles for each aliphatic compound and ionic liquid ion were also used to achieve a better understanding of the ternary systems behavior. The selectivity and the distribution ratio values were calculated by Eqs. (6) and (7). These values, for the different cation and anion combinations, are presented in Tables S2 and S3 and depicted in Figs. S1a–p, S2a–k, S3a–d and S4a–d in the Supporting Information. While Fig. S1 shows the impact of the cation family and Fig. S2 the anion nature effect, Fig. S3 shows the cation alkyl chain length and the cation symmetry influence and Fig. S4 the anion alkyl chain length impact, estimated by COSMO-RS on the mentioned parameters. Their simultaneous analysis with the σ-profiles of each compound and the COSMO-RS mixture energies, allows a better understanding of the interactions taking place and the most appropriate ionic liquid characteristics required for the thiols extraction process.

The COSMO-RS σ-profiles are represented in Figs. S5–S16 in the Supporting Information. The σ-profiles represent the charge density distribution, $p(\sigma)$, based on the virtual σ-surface, and provide information on the molecular surface polarity. The σ axis represents the surface polarity charge and has negative values for molecule positive charges and vice versa; when $\sigma < -0.0082$ e/A^2 or > 0.0082 e/A^2 there is evidence on the hydrogen-bonding ability, representing, respectively, donor and acceptor molecule regions [65].

The COSMO-RS σ-profiles for the kerosene model compounds, 1-hexanethiol and *n*-dodecane, are depicted in Fig. S5 in the Supporting Information. Both compounds show a thin and high peak, centered in the overall plot ($-0.008 < \sigma$ (e/A^2) < 0.006 and $-0.006 < \sigma$ (e/A^2) < 0.006, respectively), as a result of the non-polar and homogeneity of the charge density along the molecules chains. At this region, the dominant interactions are van der Waals forces. Being the 1-hexanethiol a more polar compound, it is also possible to observed two small peaks, at $\sigma = 0.007$ e/A^2 and $\sigma = 0.012$ e/A^2, due to the two electron concentration regions caused by the electronegative sulfur atom, and a third peak, at $\sigma = -0.009$ e/A^2, by the electron delocalization of the sulfur atom leaving the hydrogen atom partially and positively charged. Although small, these peaks indicate a slight ability to hydrogen-bond.

Based on these considerations, it is thus expectable to be able to tailor the flexible affinity of ionic liquids for thiols by changing their chemical structures. In fact, the cation and anion σ-profiles show more distinct type of interactions than the fuel model compounds. The σ-profiles of the ionic liquids cations and anions are presented in Figs. S5–S16 in the Supporting Information. In the σ-profiles plot, the positive peaks correspond, in general, to the ionic liquid anions, and the negative to the ionic liquid cation. It is also noteworthy to mention that these strength peaks can also provide information on the cation–anion cohesion forces.

Considering the σ-profile diagram of 1-hexanethiol, the most suitable ionic liquid should present a cation with a peak close to $\sigma = -0.012$ e/A^2 and an anion with a peak around $\sigma = 0.009$ e/A^2 aiming at promoting a strong interaction with the thiol. However, these thiol peaks are small and the expected hydrogen-bonding is weak. On the other hand, the van der Waals interactions between the non-polar regions of the compounds, due to the centered high peak, and misfit electrostatic interactions caused by the ionic liquid charges, will be dominant. Nevertheless, these interactions also improve the affinity of the ionic liquids to the alkane, and

consequently a decrease on the systems selectivity is further observed. Therefore, the most suitable ionic liquids should not present high peaks in the region $-0.006 < \sigma\ (e/A^2) < 0.006$.

Eqs. (1)–(3), COSMO-RS split the interaction energy into three specific energies, the misfit electrostatic energy, the hydrogen-bonding energy and the van der Waals energy, being the first two energies dependent on the σ-profiles of each compound. The third energy is only dependent on the individual atoms properties. The estimated energies can be assessed in Tables S4 and S5 in the Supporting Information, for the model feed 1-hexanethiol + *n*-dodecane and for the ternary systems ionic liquid + 1-hexanethiol + *n*-dodecane, respectively. Higher van der Waals energies are found in the model feed confirming that the interactions between these compounds are mainly due to dispersive forces, as expected. Comparing the COSMO-RS energies of 1-hexanethiol in the model mixture (Table S4) with its energies when ionic liquids are added (Table S5), it is possible to notice that strong van der Waals energies are also determined for the ionic liquid ions, which promote the main interactions between both compounds. A significant increase in the 1-hexanethiol misfit and hydrogen-bonding energies is also observed with all the ionic liquids studied, which demonstrates that these type of interactions also take place in the 1-hexanethiol and ionic liquid mixtures.

4.2.1. Predicted effect of the ionic liquid cation core

The selectivity and distribution ratio for the thiol are dependent on the ionic liquid cation structural differences as shown in Fig. S1a–p, as well as in the σ-profiles plots in Figs. S5–S15, in the Supporting Information.

COSMO-RS predicts the complete miscibility with the fuel model compounds, high distribution ratios and small selectivities for quaternary phosphonium-based ionic liquids ($[P_{666(14)}]^+$). Their long alkyl chains largely increase the van der Waals energies of the cation (Table S5k)) and promote dispersive interactions with non-polar compounds. This is consistent with the $[P_{666(14)}]$ cation σ-profile (Fig. S5), which shows a very high pronounced peak in the region $-0.008 < \sigma\ (e/A^2) < 0.006$, covering and overlapping both 1-hexanethiol and *n*-dodecane peaks.

For the acyclic guanidinium and isouronium cations, namely $[(C_1)_6Gu]^+$, $[OC_2(C_1)4iU]^+$ and $[SC_2(C_1)4iU]^+$, a high distribution ratio is observed. This is a result of these cations higher affinity for thiol. Indeed, COSMO-RS forecasts the stronger van der Waals and mild misfit energies (Tables S5i, k and l) in these species. This can also be confirmed by their σ-profiles (Fig. S6), which show a peak very close to the higher 1-hexanethiol peak related with its non-polar region, and also a part of the area of 1-hexanethiol is covered by those cations. The more negative peaks (cationic charges), at $\sigma = -0.006\ e/A^2$ for the $[(C_1)_6Gu]^+$ cation, and $\sigma = -0.007\ e/A^2$ for the $[OC_2(C_1)4iU]^+$ and $[SC_2(C_1)4iU]^+$ cations, lead to a charge delocalization allowing therefore the increase of the 1-hexanethiol partial negative charge interaction with the positive charge of the cations. The lower selectivity of these cations compared to others is also dependent on these factors that, on the other hand, improve the interaction of the ionic liquids with the linear alkane *n*-dodecane.

Comparing the guanidinium cation ($[Gu]^+$), with no alkyl groups, with the alkylated one, $[(C_1)_6Gu]^+$, the selectivity vs. distribution ratio values occur at the opposite plot region. The van der Waals energies in $[Gu]^+$ (Table S5i) are smaller when compared to $[(C_1)_6Gu]^+$ (Table S5j). In addition, the cation $[Gu]^+$ displays a much higher hydrogen bonding capacity (higher hydrogen-bonding energies and $\sigma_{HB} \ll -0.0082\ e/A^2$, Fig. S7), which fortify the cohesion between the cation and the anion and reduces the interaction with thiol compounds while making these mixtures less miscible.

For the cholinium cation ($[Ch]^+$), although with non-insignificant van der Waals and electrostatic interactions energies, the hydrogen-bonding is a very significant interaction (Table S5h). The small peak at $\sigma_{HB} = -0.017\ e/A^2$ and the more pronounced peak at $\sigma_{HB} = -0.009\ e/A^2$, (Fig. S7) reinforce the cation–anion forces and hinder the thiol interactions.

For other ringed nitrogen-based cations, the predicted values of selectivity decrease and the distribution ratio increase according to the following order: imidazolium, pyridinium, thiazolium, pyrrolidinium and quinolinium. Analyzing the COSMO-RS energies (Tables S5a–f), it is observed that for these cation-based mixtures, the dominant energies are van der Waals, followed by mild misfit and hydrogen-bonding. All of these cations show similar σ-profiles (Fig. S8) even for the non-aromatic pyrrolidinium cation and for the quinolinium cation with two aromatic groups. Comparing the σ-profiles for the various cations, it is possible to notice an increase of the peak area from the imidazolium to the pyridinium, leading to a slight increase of the van der Waals interactions and to a respective increase on the distribution ratio. Indeed, this increment in the van der Waals forces in the pyridinium-based ionic liquids fully agree with the experimental data presented before regarding the ionic liquid cation influence. The increase of the distribution ratio observed on the thiazolium cation is related with the increase of the intensity of the peak corresponding to the van der Waals interactions, resulting thus in an improved interaction with the thiol. The higher pyrrolidinium distribution ratio, when compared with these two cations, is related with the negligible hydrogen-bonding since the van der Waals and the misfit energies show lower values. This pattern also reflects lower cation–anion interactions, liberating the cation for interacting with the thiol. Regarding the quinolinium cation, it shows a large peak area that covers practically the area peak of 1-hexanethiol and thus results in its higher affinity and distribution ratios. Concluding, for these cations, both tendencies, namely the increase on the distribution ratio and the decrease on selectivity, are a result of the improvement of the interactions between both the thiol and *n*-dodecane with the ionic liquid cations, mainly due to the improvement of the van der Waals forces.

4.2.2. Predicted effect of the ionic liquid anion

The anions impact on the thiols partition predicted by COSMO-RS, namely the selectivity vs. distribution ratio for the different ionic liquid anions, is depicted in Fig. S2a–k in the Supporting Information. The COSMO-RS energies were also determined and are presented in Tables S5a–l in the Supporting Information.

The anions $[PF_6]^-$ and $[BF_4]^-$ show the highest selectivity amongst the studied anions. In addition, for both anions, a very small distribution ratio is predicted. Analyzing the COSMO-RS mixture energy values, these fluorinated anions present relative small van der Waals and hydrogen-bonging energies. Therefore, there is a very low affinity of both anions for the thiol.

For the sulfur-based anions, the COSMO-RS predicted distribution ratios and selectivities follow the order: $[CF_3SO_3]^-$, $[MeSO_4]^-$ and $[CH_3SO_3]^-$. The van der Waals and the electrostatic energies are similar in these sulfurous-based systems. In addition, all the anions display relatively low hydrogen-bonding energies. However, the highest hydrogen-bonding energy was observed for the anion $[CH_3SO_3]^-$, leading to a COSMO-RS prediction of a high distribution ratio and low selectivity with this anion. The σ-profiles of the sulfurous-based anions are shown in Fig. S10 in the Supporting Information. The $[MeSO_4]^-$ and the $[CH_3SO_3]^-$ anions present small peaks in the negative region and inside the 1-hexanethiol peak area, which further indicate weak van der Waals interactions. The $[CH_3SO_3]^-$ also presents a peak at $-0.007\ e/A^2$, that suits the 1-hexanethiol peak at $0.007\ e/A^2$, and may be responsible for the high affinity between this anion and 1-hexanethiol. The $[CF_3SO_3]^-$ shows a first

peak at 0.003 e/A^2 that covers part of the 1-hexanethiol peak, and a second peak very close to the one of the $[CH_3SO_3]^-$, at 0.014 e/A^2, due to their structural similarity. For $[(PFBu)SO_3]^-$, the same peak at 0.014 e/A^2 is found due to the $-SO_3$ group, and a higher peak is also observed at 0.001 e/A^2 covering a great part of the 1-hexanethiol peak and explaining their predicted higher distribution ratios and selectivity.

The $[CH_3CO_2]^-$ anion leads to a high distribution ratio and to a low selectivity for the thiol. This anion displays a slightly higher misfit energy when compared to van der Waals forces. In addition, significant hydrogen-bonding energies are found that are correlated with its positive peak at 0.020 e/A^2 (Fig. S11 in the Supporting Information).

Regarding the systems based on cyano-based anions ($[N(CN)_2]^-$, $[C(CN)_3]^-$ and $[B(CN)_4]^-$), their predicted distribution ratio and selectivity are not satisfactory for all the ionic liquid cations tested. Fig. S12, in Supporting Information, presents their σ-profiles where it is shown that these anions have peaks inside the 1-hexanethiol and the *n*-dodecane, at 0.004 e/A^2, 0.002 e/A^2, and 0.001 e/A^2, respectively.

For the systems studied, the anions that show a higher distribution ratio and a lower selectivity for 1-hexanethiol are: $[NTf_2]^-$, $[TOS]^-$, $[DEP]^-$, $[DBP]^-$ and $[FeCl_4]^-$. Regarding the COSMO-RS results, these anions present higher van der Waals and misfit energies when compared to smaller hydrogen-bonding energies. All these factors provide the required dispersive forces to interact with both the alkane and the thiol. From their σ-profiles (in Fig. S13 in the Supporting Information), it can be seen that most of these anions contain peaks inside the range $-0.006 < \sigma\ (e/A^2) < 0.006$, and with a large area covering part of the 1-hexanethiol and *n*-dodecane peaks. Nevertheless, additional care must be taken when combining such anions with different cations. Exceptions on their performance appear for the anions $[TOS]^-$, $[DEP]^-$ and $[DBP]^-$ if combined with the more polar cations, such as $[Gu]^+$ and $[Ch]^+$.

4.2.3. Predicted effect of the alkyl side chain length and symmetry

The influence of the alkyl chain length on the systems selectivity and distribution ratio can be observed in Figs. S3a–d and S4a–d in the Supporting Information for the imidazolium cation ($[C_n mim]^+$, with $n = 2$, 4, 6 and 8), and for the anions of the type $[RSO_4]^+$, with R = methyl (Me), ethyl (Et), butyl (Bu) and octyl (Oc), respectively. In both situations an increase in the alkyl chain length leads to an increase on the distribution ratio and to a decrease on the selectivity values. This pattern is a result of the enlargement of their non-polar region, increasing, therefore, their van der Waals interactions with the thiol.

The cation symmetry impact was evaluated for the dialkylimidazolium cation, $[C_nC_nim]^+$, with $n = 2$ and 4, and is also shown in Fig. S3. The COSMO-RS predicts a slight increase in the distribution ratio and a decrease in the selectivity, compared to the asymmetric $[C_2mim]^+$ and $[C_4mim]^+$, respectively. Moreover, the symmetry effect is positively influenced by the cation alkyl chain size. The existence of two alkyl side chains duplicates the non-polar surface available for van der Waals interactions.

The σ-profiles presented in Figs. S14–S16 in the Supporting Information also corroborate the trends observed.

4.3. Potential ionic liquids candidates

From the screening approach used here, the ionic liquids that could provide the best performance, based on their liquid–liquid equilibrium, comprise ions that are able to interact either by van der Waals interactions or with the –SH group. Nevertheless, some of the ionic liquid features that allow improved thiol-ionic-liquid interactions also lead to a higher affinity for the remaining feed compounds. Therefore, a balance between the distribution ratio and selectivity must exist. Considering the σ-profiles, an important aspect is that the ionic liquid ions should present some enveloping of the thiol peak indicative of their favorable interaction; yet, this should not be in excess to avoid the interactions with *n*-dodecane. The cation should present a peak close to $\sigma = -0.012$ e/A^2 and the anion close to $\sigma = 0.009$ e/A^2. Having these features in mind, the best ionic liquid candidates are those composed of imidazolium, pyridinium and pyrrolidium cations, with short alkyl side chains, combined with the anions $[TOS]^-$, $[DEP]^-$, $[EtSO_4]^-$ and $[CF_3SO_3]^-$. Some of them are already studied on this work.

4.3.1. Comparison between the selection of ionic liquids for aliphatic or for aromatic sulfur compounds removal from fuels

In the last years, many research works have been reported addressing the fuels desulfurization assisted by ionic liquids, aiming at finding the best ionic liquid able to perform an efficient extraction of the sulfur contaminants. These works mainly addressed the study of aromatic compounds such as thiophene, benzothiophene and dibenzothiophene [4,78]. Their interactions with the ionic liquids are quite distinct from the van der Waals forces observed with the aliphatic sulfur compounds, and consist of hydrogen bonds, CH–π bonds, and π–π interactions [48,79]. These favorable interactions promote a greater affinity and solubility on the ionic liquids than the observed for the aliphatic sulfur compounds.

Although many ionic liquids achieve an excellent extraction capacity and distribution ratios, either for aliphatic or aromatic sulfur compounds, these ionic liquids are also capable of co-extracting the fuel constituents, corresponding to lower selectivities. Therefore, as presented before and stated elsewhere [48,62,80–83], some structural features, that provide favorable interactions with the fuel hydrocarbons of the ionic liquid, should be avoided, such as the long cation alkyl side chains or anions with low polarity. By this fact, many authors, recognized the importance of the selectivity and the need of a balance between the selectivity and distribution ratio for this type of systems, in order to avoid the cross contamination of the fuel [17,25,48,52,80,84–87]. They chose to apply ionic liquids based on cations with small alkyl side chains, in order to promote higher selectivities, mainly from the imidazolium and pyridinium cation families. Regarding the anions, a greater diversity was tested and no defined pattern was identified. Various anions were mentioned as more suitable: $[N(CN)_2]^-$ [25,51], $[C(CN)_3]^-$ [20], $[B(CN)_4]^-$ [48], $[BF_4]^-$ [48], $[PF_6]^-$ [47,48], $[CF_3SO_3]^-$ [47,48], $[NTf_2]^-$ [17,47], $[CH_3CO_2]^-$ [47], $[SCN]^-$ (thiocyanate) [47,87], $[EtSO_4]^-$ [52], [DEP]- [88], among others.

Taking into account the ionic liquids' cations and anions here selected, along with the findings in this work, similarities are observed between the chosen ionic liquid features. Moreover, the feasibility of the ionic liquid based desulfurization processes for the integrated aliphatic and aromatics sulfur compounds extraction is further supported by the negligible mutual solubility between the ionic liquid and the fuel main constituents. Even so, the distribution ratios determined for both aliphatic and organic sulfur species [14,39,87,88] are, in many cases, low and unfavorable, which implies large volumes of ionic liquid for an efficient liquid–liquid extraction process. Nonetheless, since ionic liquids have negligible volatility and are chemically stable, their regeneration can be easily performed in an additional step through different techniques, as distillation, adsorption or back-extraction processes [4]. This allows its reuse in the extraction process leading to a more economic and sustainable separation process for the sulfur species removal [4].

5. Conclusions

This work aimed at studying ionic liquids as potential extracting solvents for the removal of thiols from kerosene streams to

fulfill the urgent need on lowering the sulfur content in industrial units. As a first approach, the experimental liquid–liquid equilibrium for the ternary systems composed of 1-hexanethiol + *n*-dodecane + ionic liquids was determined at 298.2 K and 313.2 K. Both imidazolium and pyridinium-based ionic liquids were investigated. Albeit the values of the distribution ratio for the tested systems are always lower than unit, these systems display a negligible mutual solubility between the ionic liquids and *n*-dodecane avoiding the solvent losses and the contamination of the hydrocarbon-rich phase.

Due to the innumerable possibilities of cation/anion combinations in ionic liquids, the COSMO-RS was evaluated in the predictive description of the experimental data. The root mean square deviations between the predicted and the experimental data are lower than 1% and prove the COSMO-RS ability to describe the phase behavior of systems involving ionic liquids, sulfur compounds and hydrocarbons. Based on this good performance, a large number of ionic liquid cations and anions was further investigated with COSMO-RS. For the separation of 1-hexanethiol from hydrocarbon mixtures, the recommended ionic liquids comprise short-alkyl chain imidazolium, pyridinium and pyrrolidium cations, combined with the $[TOS]^-$, $[DEP]^-$, $[EtSO_4]^-$ and $[CF_3SO_3]^-$ anions.

Acknowledgments

This work was financed by national funding from *Fundação para a Ciência e a Tecnologia* (FCT) through projects PTDC/QUI-QUI/121520/2010 and Pest-C/CTM/LA0011/2013. Ana R. Ferreira acknowledges the financial support from FCT and Galp Energia through the scholarship SFRH/BDE/33835/2009.

Appendix A. Supplementary material

Supplementary data associated with this article, namely experimental liquid-liquid equilibrium results, COSMO-RS estimated selectivity and distribution ratio values, COSMO-RS estimated energies and σ-profiles for all the compounds studied, can be found in the online version, at http://dx.doi.org/10.1016/j.fuel.2014.03.020.

References

[1] Song C. An overview of new approaches to deep desulfurization for ultra-clean gasoline, diesel fuel and jet fuel. Catal Today 2003;86:211–63.
[2] Srivastava VC. An evaluation of desulfurization technologies for sulfur removal from liquid fuels. Rsc Adv 2012;2:759–83.
[3] Francisco M, Arce A, Soto A. Ionic liquids on desulfurization of fuel oils. Fluid Phase Equilib 2010;294:39–48.
[4] Kulkarni PS, Afonso CAM. Deep desulfurization of diesel fuel using ionic liquids: current status and future challenges. Green Chem 2010;12:1139–49.
[5] Wang W, Wang S, Liu H, Wang Z. Desulfurization of gasoline by a new method of electrochemical catalytic oxidation. Fuel 2007;86:2747–53.
[6] Seredych M, Wu CT, Brender P, Ania CO, Vix-Guterl C, Bandosz TJ. Role of phosphorus in carbon matrix in desulfurization of diesel fuel using adsorption process. Fuel 2012;92:318–26.
[7] Mochizuki Y, Sugawara K. Selective adsorption of organic sulfur in coal extract by using metal-loaded carbon. Fuel 2011;90:2974–80.
[8] Werner S, Haumann M, Wasserscheid P. Ionic liquids in chemical engineering. Annu Rev Chem Biomol 2010;1:203–30.
[9] Liang WD, Zhang S, Li HF, Zhang GD. Oxidative desulfurization of simulated gasoline catalyzed by acetic acid-based ionic liquids at room temperature. Fuel Process Technol 2013;109:27–31.
[10] Wang JL, Zhao DS, Li KX. Extractive desulfurization of gasoline using ionic liquid based on CuCl. Petrol Sci Technol 2012;30:2417–23.
[11] Li FT, Liu Y, Sun ZM, Chen LJ, Zhao DS, Liu RH, et al. Deep extractive desulfurization of gasoline with xEt(3)NHCl center dot FeCl3 ionic liquids. Energy Fuel 2010;24:4285–9.
[12] Alonso L, Arce A, Francisco M, Rodriguez O, Soto A. Gasoline desulfurization using extraction with [C-8 mim][BF4] ionic liquid. AIChE J 2007;53:3108–15.
[13] Huang CP, Chen BH, Zhang J, Liu ZC, Li YX. Desulfurization of gasoline by extraction with new ionic liquids. Energy Fuel 2004;18:1862–4.
[14] Kuhlmann E, Haumann M, Jess A, Seeberger A, Wasserscheid P. Ionic liquids in refinery desulfurization: comparison between biphasic and supported ionic liquid phase suspension processes. Chemsuschem 2009;2:969–77.
[15] Taha MF, Atikah N, Chong FK, Shaharun MS. Oxidative desulfurization of dibenzothiophene from model oil using ionic liquids as extracting agent. Aip Conf Proc 2012;1482:258–62.
[16] de Oliveira LH, Alvarez VH, Aznar M. Liquid–liquid equilibrium in n-methyl-2-hydroxyethylammonium acetate, butanoate, or hexanoate ionic liquids plus dibenzothiophene plus n-dodecane systems at 298.2 K and atmospheric pressure. J Chem Eng Data 2012;57:744–50.
[17] Rodríguez-Cabo B, Arce A, Soto A. Desulfurization of fuels by liquid–liquid extraction with 1-ethyl-3-methylimidazolium ionic liquids. Fluid Phase Equilib 2013;356:126–35.
[18] Krolikowski M, Walczak K, Domanska U. Solvent extraction of aromatic sulfur compounds from n-heptane using the 1-ethyl-3-methylimidazolium tricyanomethanide ionic liquid. J Chem Thermodyn 2013;65:168–73.
[19] Gabric B, Sander A, Bubalo MC, Macut D. Extraction of S- and N-compounds from the mixture of hydrocarbons by ionic liquids as selective solvents. Sci World J 2013.
[20] Domańska U, Lukoshko EV, Królikowski M. Separation of thiophene from heptane with ionic liquids. J Chem Thermodyn 2013;61:126–31.
[21] Dharaskar SA, Wasewar KL, Varma MN, Shende DZ, Yoo CK. Deep removal of sulfur from model liquid fuels using 1-butyl-3-methylimidazolium chloride. Procedia Eng 2013;51:416–22.
[22] Wilfred CD, Kiat CF, Man Z, Bustam MA, Mutalib MIM, Phak CZ. Extraction of dibenzothiophene from dodecane using ionic liquids. Fuel Process Technol 2012;93:85–9.
[23] Kedra-Krolik K, Mutelet F, Moise JC, Jaubert JN. Deep fuels desulfurization and denitrogenation using 1-butyl-3-methylimidazolium trifluoromethane sulfonate. Energy Fuel 2011;25:1559–65.
[24] Wang Y, Li H, Zhu W, Jiang X, He L, Lu J, et al. The extractive desulfurization of fuels using ionic liquids based on FeCl3. Petrol Sci Technol 2010;28:1203–10.
[25] Yu GR, Li X, Liu XX, Asumana C, Chen XC. Deep desulfurization of fuel oils using low-viscosity 1-ethyl-3-methylimidazolium dicyanamide ionic liquid. Ind Eng Chem Res 2011;50:2236–44.
[26] Zhu W, Xu D, Li H, Ding Y, Zhang M, Liu H, et al. Oxidative desulfurization of dibenzothiophene catalyzed by VO(acac)(2) in ionic liquids at room temperature. Petrol Sci Technol 2013;31:1447–53.
[27] Zhu W, Wu P, Yang L, Chang Y, Chao Y, Li H, et al. Pyridinium-based temperature-responsive magnetic ionic liquid for oxidative desulfurization of fuels. Chem Eng J 2013;229:250–6.
[28] Zhang M, Zhu W, Xun S, Li H, Gu Q, Zhao Z, et al. Deep oxidative desulfurization of dibenzothiophene with POM-based hybrid materials in ionic liquids. Chem Eng J 2013;220:328–36.
[29] Pereiro AB, Tome LC, Martinho S, Rebelo LPN, Marrucho IM. Gas permeation properties of fluorinated ionic liquids. Indust Eng Chem Res 2013;52:4994–5001.
[30] Zhao PP, Zhang MJ, Wu YJ, Wang J. Heterogeneous selective oxidation of sulfides with H_2O_2 catalyzed by ionic liquid-based polyoxometalate salts. Ind Eng Chem Res 2012;51:6641–7.
[31] Li Z, Li CP, Chi YS, Wang AL, Zhang ZD, Li HX, et al. Extraction process of dibenzothiophene with new distillable amine-based protic ionic liquids. Energy Fuel 2012;26:3723–7.
[32] Zhang C, Pan XY, Wang F, Liu XQ. Extraction–oxidation desulfurization by pyridinium-based task-specific ionic liquids. Fuel 2012;102:580–4.
[33] Rodríguez-Cabo B, Rodríguez H, Rodil E, Arce A, Soto A. Extractive and oxidative–extractive desulfurization of fuels with ionic liquids. Fuel 2014;117, Part A:882–9.
[34] Nie Y, Dong Y, Bai L, Dong H, Zhang X. Fast oxidative desulfurization of fuel oil using dialkylpyridinium tetrachloroferrates ionic liquids. Fuel 2013;103:997–1002.
[35] Lu L, Cheng SF, Gao JB, Gao GH, He MY. Deep oxidative desulfurization of fuels catalyzed by ionic liquid in the presence of H_2O_2. Energy Fuel 2007;21:383–4.
[36] Yahaya GO, Hamad F, Bahamdan A, Tammana VVR, Hamad EZ. Supported ionic liquid membrane and liquid–liquid extraction using membrane for removal of sulfur compounds from diesel/crude oil. Fuel Process Technol 2013;113:123–9.
[37] Lin Y, Wang F, Zhang Z, Yang J, Wei Y. Polymer-supported ionic liquids: synthesis, characterization and application in fuel desulfurization. Fuel 2014;116:273–80.
[38] Wang F, Zhang Z, Yang J, Wang L, Lin Y, Wei Y. Immobilization of room temperature ionic liquid (RTIL) on silica gel for adsorption removal of thiophenic sulfur compounds from fuel. Fuel 2013;107:394–9.
[39] Kohler F, Roth D, Kuhlmann E, Wasserscheid P, Haumann M. Continuous gas-phase desulfurisation using supported ionic liquid phase (SILP) materials. Green Chem 2010;12:979–84.
[40] Martínez-Magadán J-M, Oviedo-Roa R, García P, Martínez-Palou R. DFT study of the interaction between ethanethiol and Fe-containing ionic liquids for desulfuration of natural gasoline. Fuel Process Technol 2012;97:24–9.
[41] Klamt A, Eckert F. COSMO-RS: a novel and efficient method for the a priori prediction of thermophysical data of liquids. Fluid Phase Equilib 2000;172:43–72.
[42] Klamt A. Summary, limitations, and perspectives. In: COSMO-RS. Amsterdam: Elsevier; 2005. p. 205–7.
[43] Diedenhofen M, Klamt A. COSMO-RS as a tool for property prediction of IL mixtures – a review. Fluid Phase Equilib 2010;294:31–8.

[44] Vega E, Lemus J, Anfruns A, Gonzalez-Olmos R, Palomar J, Martin MJ. Adsorption of volatile sulphur compounds onto modified activated carbons: effect of oxygen functional groups. J Hazard Mater 2013;258:77–83.

[45] Shah MR, Anantharaj R, Banerjee T, Yadav GD. Quaternary (liquid plus liquid) equilibria for systems of imidazolium based ionic liquid plus thiophene plus pyridine plus cyclohexane at 298.15 K: experiments and quantum chemical predictions. J Chem Thermodyn 2013;62:142–50.

[46] Anantharaj R, Banerjee T. Fast solvent screening for the simultaneous hydrodesulfurization and hydrodenitrification of diesel oil using ionic liquids. J Chem Eng Data 2011;56:2770–85.

[47] Anantharaj R, Banerjee T. COSMO-RS based predictions for the desulphurization of diesel oil using ionic liquids: effect of cation and anion combination. Fuel Process Technol 2011;92:39–52.

[48] Kumar AAP, Banerjee T. Thiophene separation with ionic liquids for desulphurization: a quantum chemical approach. Fluid Phase Equilib 2009;278:1–8.

[49] Anantharaj R, Banerjee T. Liquid–liquid equilibria for quaternary systems of imidazolium based ionic liquid plus thiophene plus pyridine plus iso-octane at 298.15 K: experiments and quantum chemical predictions. Fluid Phase Equilib 2011;312:20–30.

[50] Anantharaj R, Banerjee T. Evaluation and comparison of global scalar properties for the simultaneous interaction of ionic liquids with thiophene and pyridine. Fluid Phase Equilib 2010;293:22–31.

[51] Wilfred CD, Man Z, Chan ZP. Predicting methods for sulfur removal from model oils using COSMO-RS and partition coefficient. Chem Eng Sci 2013;102:373–7.

[52] Varma NR, Ramalingam A, Banerjee T. Experiments, correlations and COSMO-RS predictions for the extraction of benzothiophene from n-hexane using imidazolium-based ionic liquids. Chem Eng J 2011;166:30–9.

[53] Anantharaj R, Banerjee T. Thermodynamic properties of 1-ethyl-3-methylimidazolium methanesulphonate with aromatic sulphur, nitrogen compounds at T = 298.15–323.15 K and P = 1 bar. Can J Chem Eng 2013;91:245–56.

[54] Anantharaj R, Banerjee T. Aromatic sulfur–nitrogen extraction using ionic liquids: experiments and predictions using an a priori model. Aiche J 2013;59:4806–15.

[55] Anantharaj R, Banerjee T. Quantum chemical studies on the simultaneous interaction of thiophene and pyridine with ionic liquid. AIChE J 2011;57:749–64.

[56] Palomar J, Torrecilla JS, Ferro VR, Rodríguez F. Development of an a priori ionic liquid design tool. 2. ionic liquid selection through the prediction of COSMO-RS molecular descriptor by inverse neural network. Ind Eng Chem Res 2009;48:2257–65.

[57] Freire MG, Ventura SPM, Santos LMNBF, Marrucho IM, Coutinho JAP. Evaluation of COSMO-RS for the prediction of LLE and VLE of water and ionic liquids binary systems. Fluid Phase Equilib 2008;268:74–84.

[58] Freire MG, Santos LMNBF, Marrucho IM, Coutinho JAP. Evaluation of COSMO-RS for the prediction of LLE and VLE of alcohols + ionic liquids. Fluid Phase Equilib 2007;255:167–78.

[59] Freire MG, Carvalho PJ, Santos LMNBF, Gomes LR, Marrucho IM, Coutinho JAP. Solubility of water in fluorocarbons: experimental and COSMO-RS prediction results. J Chem Thermodyn 2010;42:213–9.

[60] Banerjee T, Singh MK, Khanna A. Prediction of binary VLE for imidazolium based ionic liquid systems using COSMO-RS. Ind Eng Chem Res 2006;45:3207–19.

[61] Banerjee T, Sahoo RK, Rath SS, Kumar R, Khanna A. Multicomponent liquid–liquid equilibria prediction for aromatic extraction systems using COSMO-RS. Ind Eng Chem Res 2007;46:1292–304.

[62] Ferreira AR, Freire MG, Ribeiro JC, Lopes FM, Crespo JG, Coutinho JAP. Overview of the liquid–liquid equilibria of ternary systems composed of ionic liquid and aromatic and aliphatic hydrocarbons, and their modeling by COSMO-RS. Ind Eng Chem Res 2012;51:3483–507.

[63] ASTM D3227 – Standard Test Method for (Thiol Mercaptan) Sulfur in Gasoline, Kerosine, Aviation Turbine, and Distillate Fuels (Potentiometric Method). ASTM International; 2013.

[64] Klamt A, Eckert F, Arlt W. COSMO-RS: an alternative to simulation for calculating thermodynamic properties of liquid mixtures. Annu Rev Chem Biomol 2010;1:101–22.

[65] Klamt A. COSMO-RS from quantum chemistry to fluid phase thermodynamics and drug design. Amsterdam: Elsevier; 2005.

[66] Klamt A. The COSMO and COSMO-RS solvation models. Wiley Interdiscip Rev Comput Mol Sci 2011;1:699–709.

[67] Schäfer A, Klamt A, Sattel D, Lohrenz JCW, Eckert F. COSMO implementation in TURBOMOLE: extension of an efficient quantum chemical code towards liquid systems. Phys Chem Chem Phys 2000;2:2187–93.

[68] Schäfer A, Huber C, Ahlrichs R. Fully optimized contracted Gaussian basis sets of triple zeta valence quality for atoms Li to Kr. J Chem Phys 1994;100:5829–35.

[69] Klamt A, Eckert F. COSMOtherm program (Version C3.0 Release 13.01). Leverkusen, Germany: COSMOlogic GmbH & Co. KG; 2013.

[70] Sørensen JM, Arlt W. Liquid–liquid equilibrium data collection. DECHEMA, Frankfurt: Ternary systems; 1980.

[71] Fernandes AM, Rocha MAA, Freire MG, Marrucho IM, Coutinho JAP, Santos LSMNBF. Evaluation of cation–anion interaction strength in ionic liquids. J Phys Chem B 2011;115:4033–41.

[72] Bini R, Bortolini O, Chiappe C, Pieraccini D, Siciliano T. Development of cation/anion "interaction" scales for ionic liquids through ESI-MS measurements. J Phys Chem B 2006;111:598–604.

[73] Lungwitz R, Strehmel V, Spange S. The dipolarity/polarisability of 1-alkyl-3-methylimidazolium ionic liquids as function of anion structure and the alkyl chain length. New J Chem 2010;34:1135–40.

[74] Freire MG, Carvalho PJ, Fernandes AM, Marrucho IM, Queimada AJ, Coutinho JAP. Surface tensions of imidazolium based ionic liquids: anion, cation, temperature and water effect. J Colloid Interface Sci 2007;314:621–30.

[75] Bhattacharjee A, Varanda C, Freire MG, Matted S, Santos LMNBF, Marrucho IM, Coutinho JAP. Density and viscosity data for binary mixtures of 1-alkyl-3-methylimidazolium alkylsulfates + water. J Chem Eng Data 2012;57:3473–82.

[76] Carvalho PJ, Regueira T, Santos LMNBF, Fernandez J, Coutinho JoAP. Effect of water on the viscosities and densities of 1-butyl-3-methylimidazolium dicyanamide and 1-butyl-3-methylimidazolium tricyanomethane at atmospheric pressure†. J Chem Eng Data 2009;55:645–52.

[77] Anantharaj R, Banerjee T. COSMO-RS-based screening of ionic liquids as green solvents in denitrification studies. Ind Eng Chem Res 2010;49:8705–25.

[78] Hansmeier AR, Meindersma GW, de Haan AB. Desulfurization and denitrogenation of gasoline and diesel fuels by means of ionic liquids. Green Chem 2011;13:1907–13.

[79] Lu RQ, Lin J, Qu ZQ. Theoretical study on interactions between ionic liquids and organosulfur compounds. Comput Theor Chem 2012;1002:49–58.

[80] Rodriguez H, Francisco M, Soto A, Arce A. Liquid–liquid equilibrium and interfacial tension of the ternary system heptane plus thiophene + 1-ethyl-3-methylimidazolium bis(trifluoromethanesulfonyl)imide. Fluid Phase Equilib 2010;298:240–5.

[81] Alonso L, Arce A, Francisco M, Soto A. Phase behaviour of 1-methyl-3-octyli.midazolium bis[trifluoromethylsulfonyl]imide with thiophene and aliphatic hydrocarbons: the influence of n-alkane chain length. Fluid Phase Equilib 2008;263:176–81.

[82] Alonso L, Arce A, Francisco M, Soto A. Liquid–liquid equilibria for [C(8)mim][NTf(2)] + thiophene + 2,2,4-trimethylpentane or plus toluene. J Chem Eng Data 2008;53:1750–5.

[83] Alonso L, Arce A, Francisco M, Soto A. Solvent extraction of thiophene from n-alkanes (C7, C12, and C16) using the ionic liquid [C8mim][BF4]. J Chem Thermodyn 2008;40:966–72.

[84] Alonso L, Arce A, Francisco M, Soto A. Thiophene separation from aliphatic hydrocarbons using the 1-ethyl-3-methylimidazolium ethylsulfate ionic liquid. Fluid Phase Equilib 2008;270:97–102.

[85] de Oliveira LH, Aznar M. Phase equilibria in ionic liquids plus dibenzothiophene plus n-dodecane systems. Ind Eng Chem Res 2011;50:2289–95.

[86] Cheruku SK, Banerjee T. Liquid–liquid equilibrium data for 1-ethyl-3-methylimidazolium acetate-thiophene-diesel compound: experiments and correlations. J Solution Chem 2012;41:898–913.

[87] Holbrey JD, Lopez-Martin I, Rothenberg G, Seddon KR, Silvero G, Zheng X. Desulfurisation of oils using ionic liquids: selection of cationic and anionic components to enhance extraction efficiency. Green Chem 2008;10:87–92.

[88] Jiang XC, Nie Y, Li CX, Wang Z. Imidazolium-based alkylphosphate ionic liquids – a potential solvent for extractive desulfurization of fuel. Fuel 2008;87:79–84.